VERIFICATION OF A PLANE STRAIN MODEL FOR THE ANALYSIS OF ENCASED GRANULAR COLUMNS

Iman Hosseinpour [1*], Mario Riccio [2], and Marcio S.S. Almeida [2]

ABSTRACT

A simplified 2D plane strain finite element analysis was applied to predict the field response of a test embankment on geotextile-encased granular columns. Numerical simulation was carried out by transforming the granular columns into the equivalent walls with the angle of friction increased accordingly to account for the coating influence of the geotextile. The purpose of increasing the friction angle of the granular columns was to indirectly consider the influence of the geotextile encasement originally proposed by Raithel and Henne (2000). Unlike the axisymmetric unit cell model, the geotextile hoop tensile strains cannot be calculated when using a 2D plane strain model. However, use of the typical axisymmetric unit cell model is questionable since the lateral spreading of backfill and its supporting foundation cannot be simulated. Comparison with field measurements showed that using the equivalent friction angle for the granular columns in the plane strain model, allowed the contribution of the geotextile encasement to be simulated reasonably well.

Key words: Soft soil, encased granular column, geotextile, plane strain analysis, embankment.

1. INTRODUCTION

Granular columns are commonly used to reduce the settlement, increase the load-bearing capacity, and accelerate the construction of embankments on soft clay (Mitchell and Huber 1985). In very soft clay (undrained shear strength, S_u < 15 kPa), encasing the granular column with geosynthetics material significantly reduces column bulging, decreases the overall deformations of the soft soil and improves the stability of the embankment (Gniel and Bouazza 2010; Almeida and Marques 2013). Meanwhile, geosynthetic encasement prevents intermixing of the soft clay particles into the granular aggregates, and subsequently the drainage capacity of the granular material remains intact (Raithel *et al.* 2005; Murugesan and Rajagopal 2010).

For the geosynthetic encased-granular column a 2D axisymmetric model, consisting of a single encased column and its surrounding soft soil, can be simply used to perform the numerical analysis (Murugesan and Rajagopal 2006; Malarvizhi and Ilamparuthi 2007; Khabbazian *et al.* 2010; Dash and Bora 2013; Almeida *et al.* 2013; Hosseinpour *et al.* 2014; Hasan and Samadhiya 2016; Geng *et al.* 2017; Rajesh 2017). The typical axisymmetric unit cell model with horizontally fixed side boundary conditions underestimates the horizontal deformation of foundation soil and geotextile encasement and thus both the soil and geotextile strains. Although a 3D analysis is more appropriate for this type of geosynthetic application, a 2D plane strain model might also be used to predict the horizontal deformation of the foundation soil underneath the embankment. A simplified methodology for a 2D plane strain analysis of granular columns without encasement was proposed by Tan *et al.* (2008) in which a unit cell was converted into a wall in order to obtain the equivalent plan strain column width. Selection of the geotextile stiffness based on a 2D plane strain model is inherently impossible; thus its confining support is ignored and consequently the computed total deformations are higher than the actual values.

This paper presents a plane strain analysis of geotextile-encased granular columns whose the geotextile encasement support was indirectly taken into account. The plane strain transformation was conducted by converting the granular columns into the equivalent walls. The confining stress of the encasement was then simulated by replacing the original friction angle of the column fill material by an increased equivalent friction angle. The numerical results were compared with measurements available from a full-scale load test in order to verify whether the combined conversion procedure could suitably predict the actual behavior of the reinforced soft ground.

2. CASE CONSIDERED FOR NUMERICAL ANALYSIS

Data provided by a stage constructed test embankment on very soft clay were used to perform the plane strain analysis (Almeida *et al.* 2015). As illustrated in Fig. 1, the supporting clayey foundation comprises a soft clay layer with an overall thickness of around 8.0 m overlying stiff clay. The upper crust layer consists of a working platform, about 1.60 m-thick, provided to improve the ground surface for stable construction activities as well as drainage of water during consolidation. Based on Fig. 1(a), the submerged unit weight (γ') varies between 3.5 and 4.0 kN/m³ for soft clay I, representing typical values of very soft clay in the west of Rio de Janeiro state (Baroni and Almeida 2012). The compressibility ratio, defined as $CR = C_c / (1 + e_0)$,

[1] Assistant Professor (corresponding author), Department of Civil Engineering, University of Guilan, Rasht, Iran (e-mail: i.hosseinpour@gmail.com).

[2] Associate Professor, Faculty of Engineering, Federal University of Juiz de Fora, Juiz de Fora, MG, Brazil.

[3] Professor, Graduate School of Engineering, Federal University of Rio de Janeiro, Rio de Janeiro, RJ, Brazil.

where C_c is the compressibility index and e_0 is the initial void ratio, obtained from the oedometer tests is also presented in Fig. 1(b), and the average *CR* value is equal to 0.27 in soft clay I, indicating the high compressibility of this layer. The natural water level is located 1.2 m below the ground surface.

The soft clay foundation was stabilized by 36 geotextile-encased granular columns installed with 2.0 m center-to-center spacing in a square array. The diameter and length of the granular columns were 80 cm and 11 m, respectively. The construction of columns was performed in 2008, while the site investigation, instrumentation and monitoring were carried out in 2012. This four year period was more than enough to dissipate the effect of column installation on the embankment settlement, and thus that is not considered in the current study. The granular columns were encased by woven geotextile with a tensile stiffness (*J*) and maximum allowable ring tensile force equal to 1,750 kN/m and 95 kN/m, respectively. Also a basal geogrid (*J* = 2,200 kN/m) was placed at the embankment base to control the overall deformations of the soft clay foundation.

Ground instrumentation was carried out to measure the settlement, total vertical stresses below the embankment, excess pore pressures in soft soil, horizontal deformation beneath the embankment, and hoop strains in the geotextile encasement; however the latter are not discussed in this study as they are out of the scope of the plane strain analysis. The embankment side view with the ground reinforced by geotextile-encased granular columns is shown in Fig. 2 along with the instrumentation employed to verify the numerical results. The test embankment was constructed in four load increments, over 65 days, with consolidation intervals between the loading stages. The final height of the embankment was 5.3 m, which is equivalent a total vertical stress of 150 kPa. Details of the loading stages and consolidation intervals are given in Table 1.
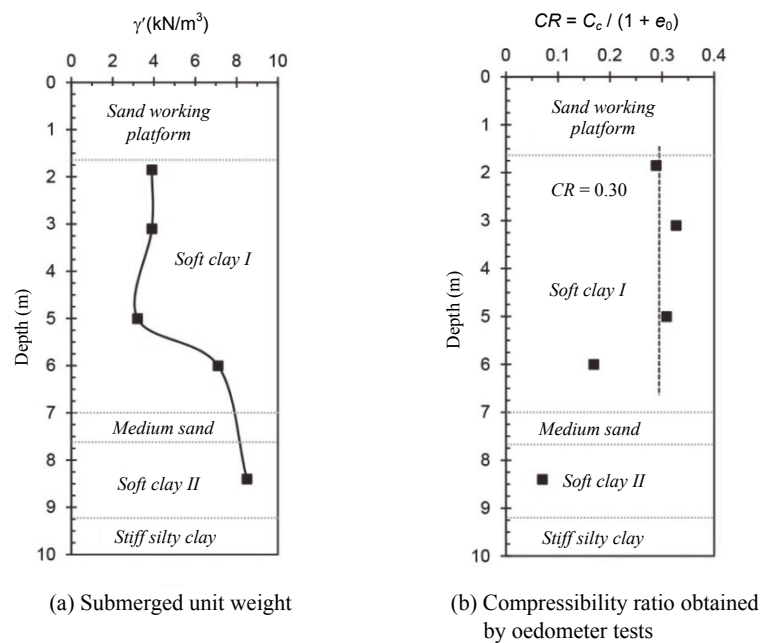

| (a) Submerged unit weight | (b) Compressibility ratio obtained by oedometer tests |

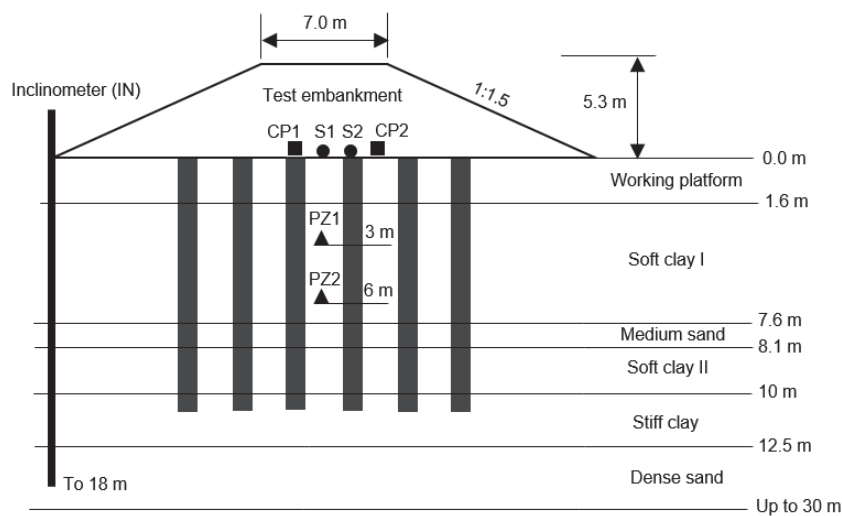**Fig. 1   Soft clay properties**

Fig. 2   Embankment side view and position of instruments

Table 1   Details of the embankment stage construction

Loading stage	Loading duration (days)	Consolidation period (days)	In-situ density of fill material, γ_n (kN/m^3)
1	3	10	27.7
2	2	32	28.3
3	2	14	27.9
4	2	180	27.1

Table 2   Material parameters used in finite element analysis of the test embankment

Material properties and constitutive models	γ_{sat} (kN/m^3)	k_h (m/d)	k_v (m/d)	ϕ' (^{o})	ϕ'_{sub} (^{o})	c' (kPa)	E' (MPa)	C_c (-)	C_s (-)
Embankment (MC)	28	1.0	1.0	45	–	0	53	–	–
Granular column (MC)	20	10	10	40	66	0	80	–	–
Soft clay I (SS)	14.4	1.6×10^{-5}	5.2×10^{-6}	26	–	4	–	0.98	0.084
Soft clay II (SS)	16.8	9.7×10^{-6}	4.8×10^{-6}	28	–	6	–	0.13	0.025
Stiff silty clay (SS)	17.8	3.3×10^{-2}	1.6×10^{-2}	30	–	12	5.5	0.09	0.0081
Working platform (MC)	19.7	0.6	0.6	33	–	3	12	–	–
Medium sand (MC)	18.5	0.5	0.5	30	–	0	22	–	–
Dense sand (MC)	20	1.0	1.0	38	–	0	30	–	–

(MC = Mohr-Coulomb model; SS = Soft Soil model)

3.   NUMERICAL SIMULATION

The 2D plane strain numerical analysis was performed using PLAXIS finite element code (Brinkgreve and Vermeer 2012) in which 15-node triangular elements were selected to simulate the soil clusters. The pre-defined geogrid element, available in PLAXIS, was used to model both the basal geogrid and the geotextile encasement which is a slender structure with an axial stiffness and can only sustain tensile force as axial strain occurs. The geotextile encasement was modeled as linear-elastic material by perfectly bonding to the adjacent soil. Several studies showed that the assumption of a perfect interface adherence in working stress conditions results in a reasonable agreement between calculated values and measured data (Hatami and Bathurst 2005; Mirmoradi and Ehrlich 2015). Fine mesh generation was adopted for the whole of the model to provide an accurate calculation of the deformations and stresses. Considering the boundary fixities, the model was restricted to deform horizontally on the vertical sides (*i.e.*, roller boundaries) while being fully fixed along the base. Although the present test embankment is inherently a 3D problem, the plane strain idealization can be applied to the profile passing through the centerline of the embankment where the instruments are actually concentrated.

The behaviour of the soft clay layers was simulated using the modified Cam-Clay model, introduced as a Soft Soil (SS) model in PLAXIS which adequately takes into account the compressibility parameters and initial volumetric state of the soft soil layers in the calculation. The SS model properties were determined from a careful site investigation performed prior to the embankment construction including Standard Penetration Test (SPT), Cone Penetration Test (CPTu), and Vane Shear Test (VST) as well as complementary laboratory testing as reported in Hosseinpour *et al.* (2017). The embankment filling material, sand layers and granular column were modeled using a linear elastic-perfectly plastic model with the Mohr-Coulomb (MC) failure criterion. The material properties used in the numerical analysis are presented in Table 2 and are similar to the typical values recommended by well-established works in the literatures (*e.g.*, Briaud 2013; Robertson 2006).

4.   ENCASED COLUMN CONVERSION

As shown in Fig. 3, the axisymmetric to plane strain conversion was performed according to the methodology proposed by Tan *et al.* (2008), which was also successfully used by Almeida *et al.* (2014). In this method, the granular columns are simulated by an equivalent plane strain wall in which half of the column width is determined by:

$$b_c = B \frac{r_c^2}{R^2} \tag{1}$$

where

r_c =   radius of the column

B =   half of the plane strain influence area

R =   radius of the unit cell

The relationship between R and B is given by the equation based on the equivalent total area and columns pattern as follows (Barron 1948):

(a) Layout of granular columns　　　(b) Axi-symmetric unit cell　　(c) Converted plane strain model

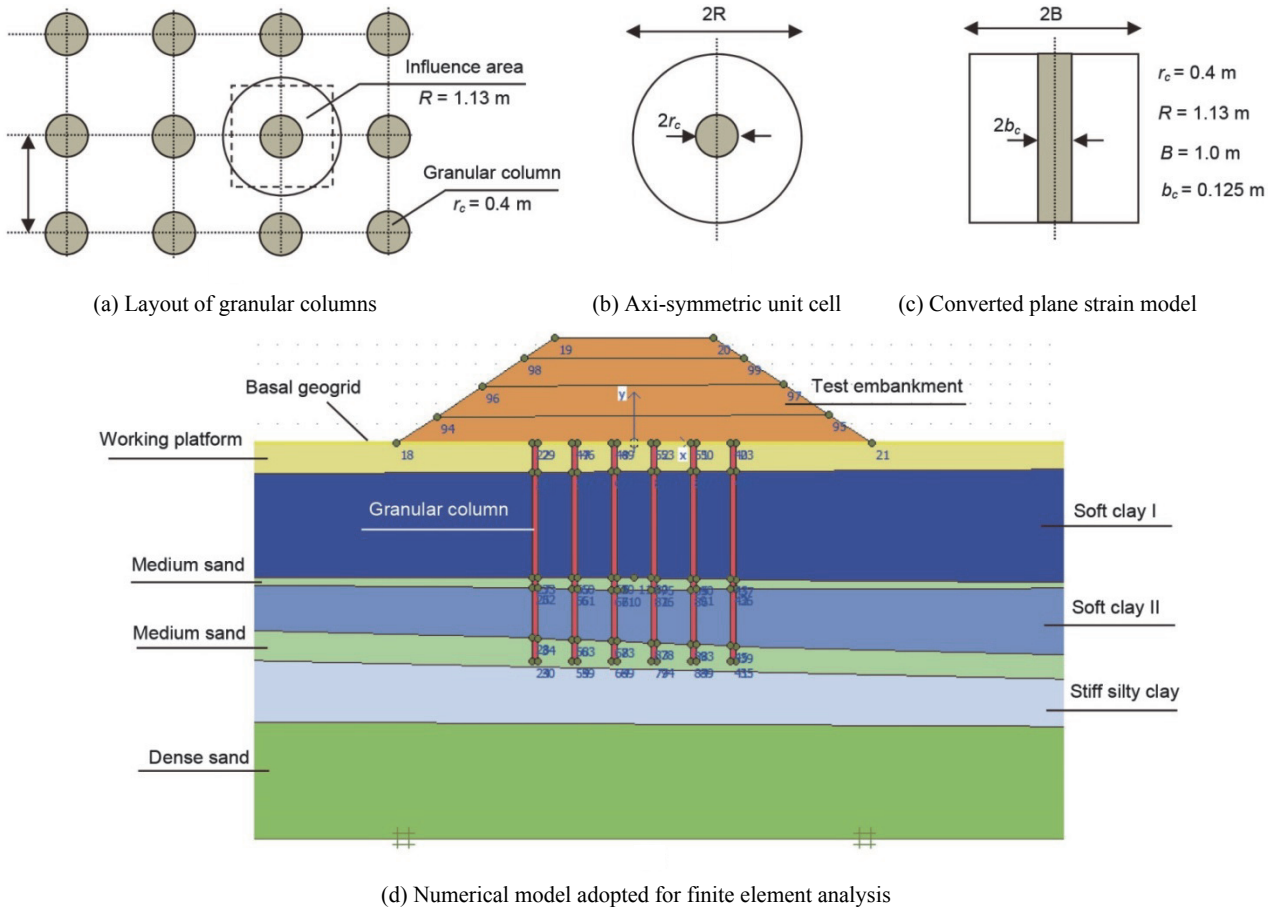(d) Numerical model adopted for finite element analysis

Fig. 3　Plane strain configuration of the test embankment

$$R = 1.13B \tag{2}$$

For the given diameter and arrangement of columns, the equivalent plane strain width (*i.e.*, $2b_c$) is calculated as 0.25 m. This approach, however, is not calibrated for the influence of the confining support provided by the geosynthetic encasement, and thus the increase of column strength and subsequent settlement reduction are not taken into account.

The theoretical method proposed by Raithel and Henne (2000) is used to account for the contribution of the geosynthetic encasement in which the friction angle of the granular columns (ϕ') is replaced by an increased friction angle (ϕ'_{sub}). This formulation is derived from Mohr's circle of stresses assuming the equilibrium of the horizontal stresses:

$$\sigma_{3,s} + \Delta\sigma_{3,geo} = \sigma_{3,c} \tag{3}$$

where $\sigma_{3,s}$ and $\sigma_{3,c}$ are respectively the inner horizontal stresses in the soil and granular column, and $\Delta\sigma_{3,geo}$ corresponds to the confining stress offered by the geosynthetic encasement. The relationship between the major and minor principle stresses ($\sigma_{1,c}$ and $\sigma_{3,c}$) in the inner part of the column considering zero cohesion is:

$$\sigma_{1,c} = \sigma_{3,c} \times \frac{1+\sin\phi'}{1-\sin\phi'} \tag{4}$$

According to Eq. (3), when using the geosynthetic encasement, the horizontal stress in the granular column $\sigma_{3,c}$ is equal to the summation of the geosynthetic confining stress $\Delta\sigma_{3,geo}$ and

the soil horizontal stress $\sigma_{3,s}$. Accordingly, Eq. (4) can be written as a function of an equivalent (or substitute) friction angle:

$$\sigma_{1,c} = (\sigma_{3,s} + \Delta\sigma_{3,c}) \times \frac{1+\sin\phi'_{sub}}{1-\sin\phi'_{sub}} \tag{5}$$

By developing Eqs. (4) and (5), the equivalent friction angle is calculated considering the effect of the confinement provided by the geosynthetic encasement:

$$\sin\phi'_{sub} = \frac{\dfrac{1+\sin\phi'}{1-\sin\phi'} + \dfrac{\Delta\sigma_{3,geo}}{\sigma_{3,c}} - 1}{\dfrac{1+\sin\phi'}{1-\sin\phi'} - \dfrac{\Delta\sigma_{3,geo}}{\sigma_{3,c}} + 1} \tag{6}$$

It is noted that the values of the horizontal stresses are simply determined by a preliminary axisymmetric analysis (Hosseinpour *et al.* 2015) for which a single encased granular column and its area of influence is analyzed. These horizontal stresses basically vary along the depth therefore their average values are used for calculation of the substitute friction angle. The use of Eq. (6) and replacement of the values of the horizontal stresses obtained from the axisymmetric analysis yields an equivalent friction angle (ϕ'_{sub}) equal to 66° for the granular column in the plane strain analysis.

5. NUMERICAL RESULTS AND FIELD OBSERVATIONS

The results obtained from the plane strain analysis were compared with data provided by the field monitoring. The instruments were placed at the embankment centerline, thus allowing a comparison with the plane strain model passing along the center of the test embankment. The main aspects compared were the settlement, total vertical stresses, horizontal deformation beneath the embankment toes, and excess pore pressures as discussed below.

5.1 Measured and Predicted Settlements

Figure 4 shows variations of the settlement on the top of the surrounding soft soil (measured by S1) and on the top of the encased column (measured by S2) both at the embankment base. It is observed that the settlements on top of both the encased column and the surrounding soil increased remarkably in the loading stage following a continuous increase during the consolidation period. It can be seen that the settlements computed using the equivalent friction angle (*i.e.*, with encasement effect) predicted the measured values fairly well, particularly the one measured on the top of the surrounding soil. However, the settlement computed using the original column friction angle (*i.e.,* without the encasement effect) was somewhat higher than the measured one. In fact, the equivalent friction angle increases the stiffness of the granular column resulting in smaller column radial deformation; subsequently the settlement is lower under the equal applied load. As observed, use of the geosynthetic-equivalent friction angle appears to be a suitable method for estimation of the settlement of the embankment over geotextile-encased granular columns in the section crossing the embankment centerline.

5.2 Measured and Predicted Total Vertical Stresses

In Fig. 5, the total vertical stresses on the top of the encased column (measured by CP2) and surrounding soil (measured by CP1) are compared with the results of plane strain analysis, and good agreement between the measured and computed values is reached. The greater total vertical stress supported by the encased column is due to the soil arching, which causes the embankment applied load to be transferred more directly to the top of the encased granular column.

As can be seen, the total vertical stresses increased when the embankment height increased, but this trend is much more pronounced for the encased column. Unlike the construction stages, the total vertical stress on the surrounding soil reveals a different behavior during the consolidation period. The increase in post-construction soil arching is attributed to the reduction of the soft soil stiffness from undrained to drained conditions, reducing the total vertical stress sustained by soft soil, and thus the soil arching progressed during post-construction. It is also observed that, in general, the use of the geosynthetic-equivalent friction angle (*i.e.,* with the encasement effect) predicted the development of the total vertical stresses on both the encased column and the surrounding soil reasonably well.

5.3 Soil Horizontal Deformation

The horizontal deformations of the foundation soil at the embankment toes measured by inclinometer IN were compared to the simulated results. Figure 6 shows the profile of the horizontal deformations at the end of construction (*i.e.*, on the 65th day) and at the end of the monitoring time (*i.e.*, on the 240th
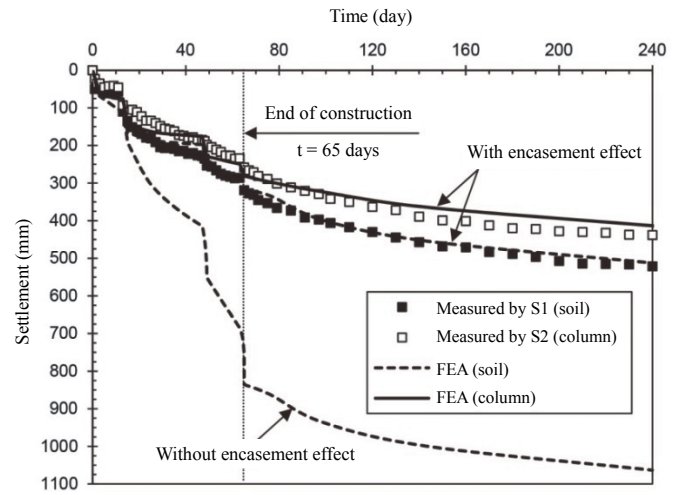

Fig. 4   Measured and predicted (FEA) settlements vs. time with and without encasement effect
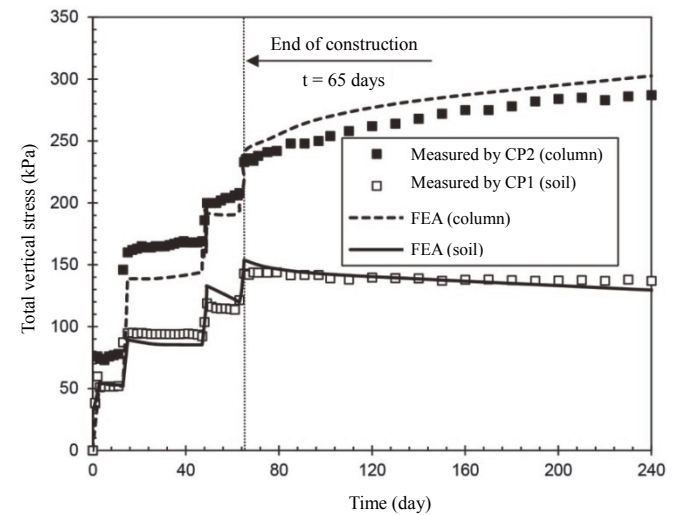

Fig. 5   Measured and predicted (FEA) total vertical stresses considering encasement effect (using equivalent friction angle)

day). It is observed that the horizontal deformations increased during the post-construction phase as the excess pore pressure dissipated. The maximum horizontal deformation of 100 mm measured after embankment construction increased up to 150 mm at the end of the monitoring period.

Horizontal deformations predicted by the equivalent friction angle showed a reasonable agreement with measurements beneath a depth of 3.0 m, particularly with regard to the magnitude of the maximum values. However, the maximum soil horizontal deformation computed using the original friction angle (*i.e.*, without the encasement effect) was as much as about three to five times greater than the values measured at the end of construction and end of the monitoring time, respectively. Figure 7 demonstrates the distribution of the soil horizontal deformation with and without the encasement effect. A larger column radial deformation is observed when the geotextile confining support is ignored, resulting in a higher soil horizontal deformation. Concentration of the horizontal strains beneath the embankment toes, as shown in Fig. 7(b), is clear evidence of the embankment lateral spreading that takes place when the geotextile encasement is not taken into account.
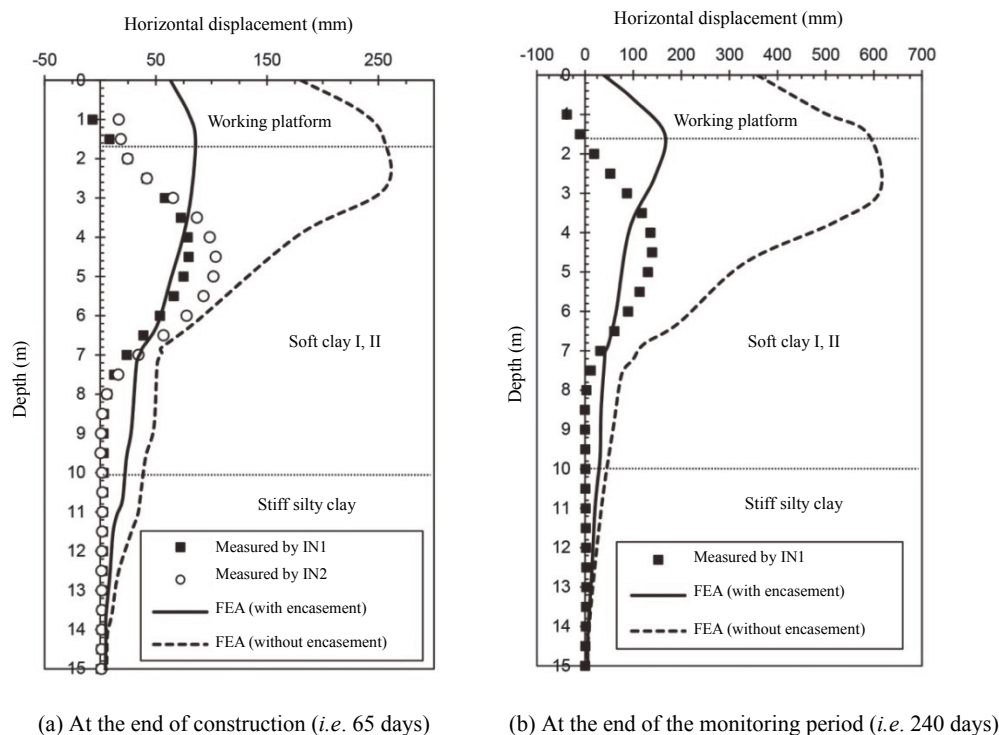
(a) At the end of construction (*i.e.* 65 days)   (b) At the end of the monitoring period (*i.e.* 240 days)

Fig. 6   Measured and predicted (FEA) soil horizontal deformation

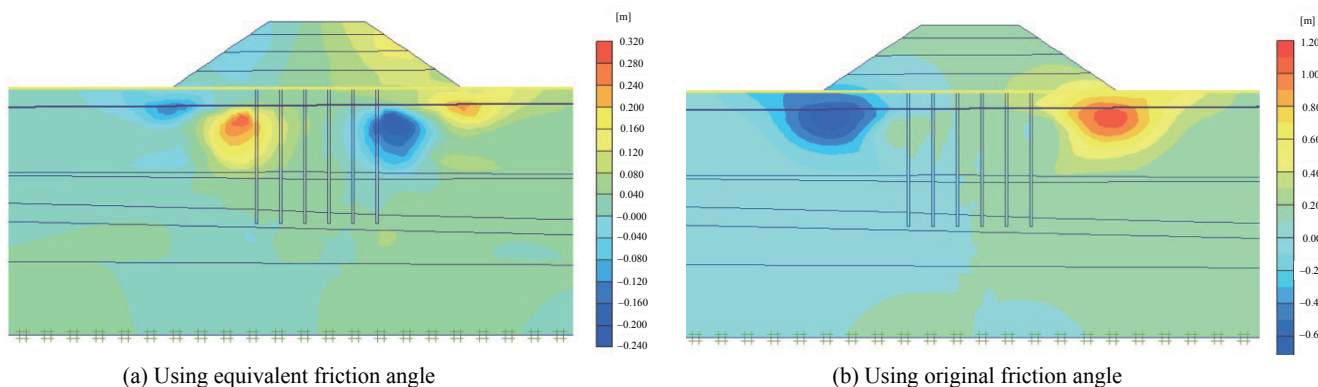(a) Using equivalent friction angle   (b) Using original friction angle

Fig. 7   Distribution of the incremental horizontal deformation at the end of the monitoring time

Generally, the use of the geosynthetic-equivalent friction angle resulted in very good computation of the soil horizontal deformation occurring beneath the embankment toes. However, the computed values were over-predicted in the upper 3.0 m. The soil anisotropy might be the reason underlying the difference between the measured and predicted horizontal deformations in this zone. In any case, it is relatively common to obtain overall good agreement between observations and numerical predictions in terms of vertical deformation and pore pressure, but not horizontal displacement (Almeida *et al*. 1986).

5.4   Measured and Predicted Excess Pore Pressures

Variations of the excess pore pressures measured by piezometers PZ1 and PZ2, both installed below the embankment centerline but at different depths, are compared to the simulated values in Fig. 8. As shown the excess pore pressure increased sharply during load application followed by partial dissipation until the next load

application. It can be seen that the geosynthetic-equivalent friction angle approach estimated the pore pressure build up reasonably well and predicted its dissipation to some extent. Using the original friction angle of the column (*i.e.*, without the encasement effect), however, resulted in a greater maximum excess pore pressure and a longer dissipation time compared to the measurement. The faster dissipation of the excess pore pressure is an indirect influence of using of the equivalent friction angle on the total stress distribution below the embankment base. In fact, the increased angle of friction increases the shear strength of the granular column causing a higher portion of the embankment total load to be carried by the granular columns; consequently the total vertical load transferred to the soil decreases. The lower total vertical load acting on soil causes the maximum excess pore pressure and time required for settlement stabilization to decreases.

For further clarification, the distribution of the total vertical stress underneath the embankment at the end of the monitoring time is demonstrated in Fig. 9. It is seen that the use of the geosynthetic-equivalent friction angle caused the total vertical stress
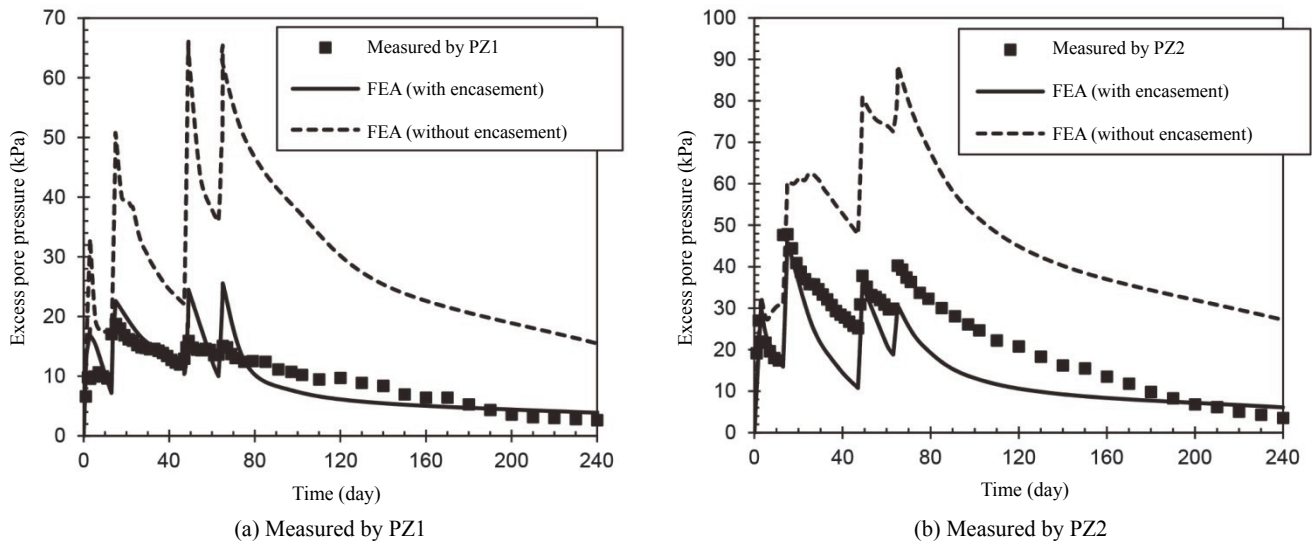
(a) Measured by PZ1   (b) Measured by PZ2

Fig. 8   Variations of the measured and predicted (FEA) excess pore pressures with and without encasement

(a) Using column original friction angle   (b) Using geosynthetic-equivalent friction angle
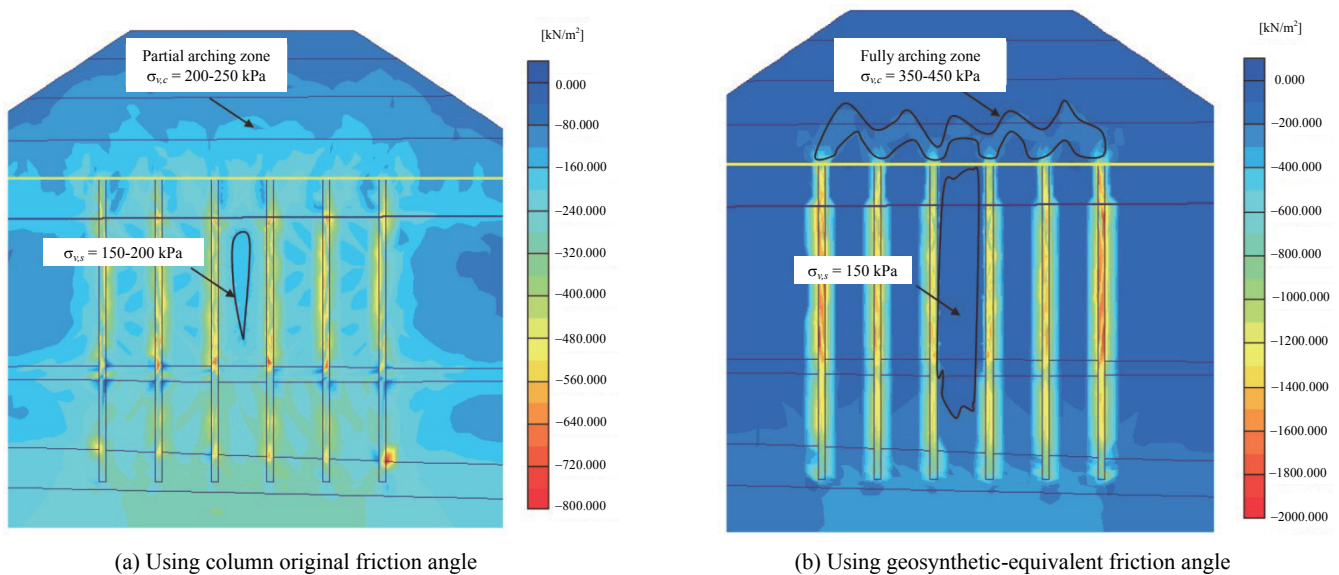
Fig. 9   Distribution of the total vertical stresses in the encased column ($\sigma_{v,c}$) and soft soil ($\sigma_{v,s}$) at the end of monitoring period

in the soft clay to decrease and inversely the total vertical load supported by the encased columns increased. In other words, the contribution of the geotextile encasement enhanced the load transfer mechanism through the soil arching over the granular columns. This confirms that the simulation of the encasement effect using the equivalent friction angle approach predicted the variations of the excess pore pressures well at the same depth where the piezometers were installed.

5.5   Stability Analysis of Embankment

Stage construction is a common method employed for the embankment construction when the soft foundation does not provide enough shear strength to prevent failure. The consolidation of the foundation following each stage of construction progressively increases the shear strength of the foundation (Almeida *et al.* 1985). In order to verify the stable performance of the test embankment, a *c*-phi reduction stability analysis was performed

to evaluate the factor of safety of the test embankment during two consecutive stages: Just after load application, and just before the next load application. Meanwhile, the stability analysis was conducted using the original column friction angle to assess the influence of the encasement on the factor of safety of the test embankment.

The results of the stability analysis of the test embankment are summarized in Fig. 10 in plots of the factor of safety (FS) against the height of embankment. Regardless of the geotextile influence, it is seen that the minimum factor of safety is reached just after the load application when the excess pore pressure in the clayey foundation is maximal (see Fig. 11(a)). Upward trends for the constant height of the embankment denote an increase in the factor of safety during the consolidation interval following the loading stage. This increase is due to the increase in shear strength of the soft clay due to dissipation of excess pore pressure, as illustrated in Fig. 11(b). As expected, the largest improvement is seen for loading stage 4, which had a consolidation period of

about six months, followed by loading stage 2, which had a longer consolidation interval (*i.e.*, 35 days) than the loading stages 1 and 3. With regard to the influence of the geotextile encasement, a significant improvement in the factor of safety was reached when the geosynthetic-equivalent friction angle was used. It can also be seen that when the geotextile effect was ignored, the test embankment failed in loading stage 3 due to the insufficient shear strength of the soft foundation.
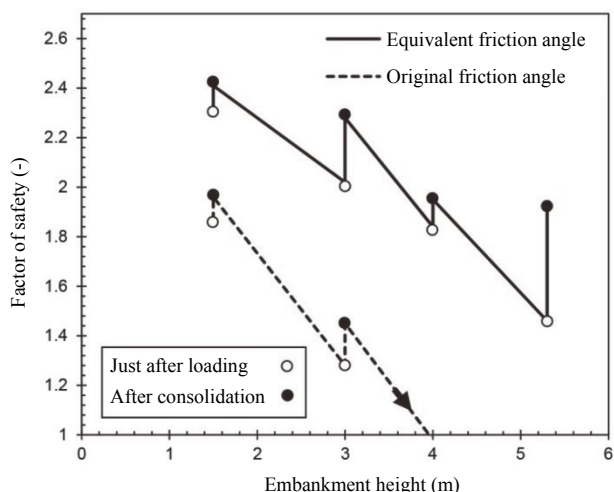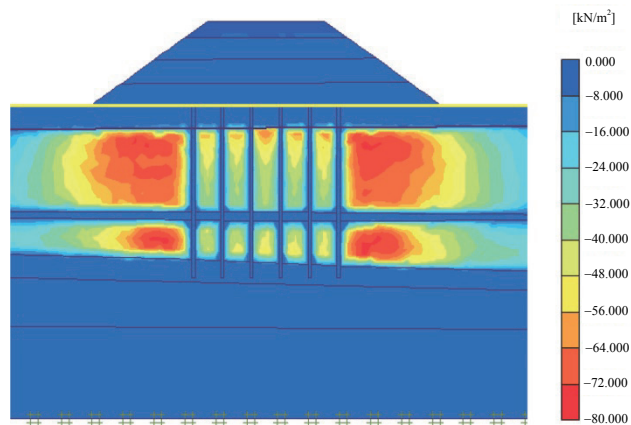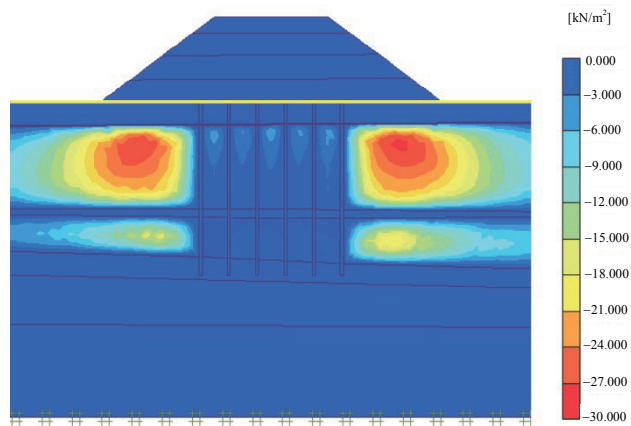

Fig. 10   Predicted factor of safety of the test embankment during construction and consolidation stages

(a) End of construction

(b) End of monitoring period

Fig. 11   Distribution of excess pore pressure

6.   CONCLUSIONS

Two-dimensional plane strain analysis was used to simulate the behavior of the geotextile-encased columns supporting the embankment and the results were compared with field measurements. The main results are as follows:

- Unlike axisymmetric analysis, the plane strain model can be used to predict the soil horizontal deformation beneath the embankment. The numerical results showed that the use of the geosynthetic-equivalent friction angle simulated the maximum values of the horizontal deformation fairly well during both construction and consolidation periods.

- The use of the geosynthetic-equivalent friction angle caused the columns to support a greater total applied stress and thus the total vertical stress in soft clay decreased; subsequently the maximum excess pore pressure upon load application and the time taken for settlement stabilization decreased significantly.

- The results of the stability analysis showed that the safety factor was a minimal just after loading was performed when the excess pore pressure was a maximal. The safety factor then increased during the consolidation stages, when the undrained strength of the foundation soil increased. Consideration of the encasement effect improved the factor of safety remarkably, while the embankment failed in loading stage 3 when the influence of the encasement was ignored.

- Although plane strain analysis is a suitable tool to determine the soil horizontal deformation and to perform safety analysis, it can compute neither the radial strain in granular columns nor the geosynthetic hoop stress, for which axisymmetric unit cell analysis has to be performed.

- The present plane strain idealization can only be applied to a profile that passes through the central area of the embankment, which has an equal number of the columns either side of the centerline. Indeed, the results of analyses such as those performed by the authors are limited to the response along such a centerline.

NOTATIONS

B	Half of equivalent plane strain influence area (m)
b_c	Half of plane strain column width (m)
c'	Effective cohesion (kPa)
C_c	Compressibility index (-)
C_s	Swelling index (-)
d_c	Column diameter (m)
E'	Drained elastic modulus (kPa)
e_0	Initial void ratio (-)
J	Geosynthetic tensile stiffness (kN/m)
k_h	Coefficient of horizontal permeability (m/d)
k_v	Coefficient of vertical permeability (m/d)

R	Diameter of the unit cell (m)
r_c	Column radius (m)
S	Columns center-to-center spacing (m)
S_u	Undrained shear strength (kPa)
z	Depth (m)
Δu	Excess pore water pressure (kPa)
$\Delta\sigma_{3,geo}$	Geosynthetic confining stress (kPa)
ϕ'	Effective friction angle (°)
ϕ'_{sub}	Equivalent friction angle (°)
γ_n	In-situ unit weight (kN/m^3)
γ_{sat}	Saturated unit weight (kN/m^3)
$\sigma_{3,c}$	Horizontal stress from column (kPa)
$\sigma_{3,s}$	Horizontal stress from surrounding soil (kPa)
$\sigma_{v,c}$	Total vertical stress on column (kPa)
$\sigma_{v,s}$	Total vertical stress on surrounding soil (kPa)

REFERENCES

Almeida, M.S.S. and Marques, M. (2013). *Design and Performance of Embankments on Very Soft Soils*. Taylor and Francis, London, UK.

Almeida, M.S.S., Davies, M.C.R., and Parry, R.H.G. (1985). "Centrifuge tests of embankments on strengthened and unstrengthened clay foundations." *Geotechnique*, **35**(4), 425–441.

Almeida, M.S.S., Britto, A.M., and Parry, R.H.G. (1986). "Numerical modelling of a centrifuged embankment on soft clay." *Canadian Geotechnical Journal*, **23**(2), 103–114.

Almeida, M.S.S., Hosseinpour, I., and Riccio, M. (2013). "Performance of a geosynthetic-encased column (GEC) in soft ground: Numerical and analytical studies." *Geosynthetics International*, **20**(4), 252–262.

Almeida, M.S.S., Hosseinpour, I., Riccio, M., and Alexiew, D. (2015). "Behaviour of geotextile-encased granular columns supporting test embankment on soft deposit." *Journal of Geotechnical and Geoenvironmental Engineering*, ASCE, **141**(3), 04014116.

Almeida, M.S.S., Lima, B., Riccio, M., Jud, H., Cascao, M., and Roza, F. (2014). "Stone columns field test: Monitoring data and numerical analyses." *Geotechnical Engineering, Journal of the SEAGS & AGSSEA*, **45**(1), 103–112.

Baroni, M. and Almeida, M.S.S. (2012). "In situ and laboratory parameters of extremely soft organic clay deposits." *Proceeding of the 4th Conference on Site Characterization ISC 4*, Volume 2, Coutinho & Mayne, Eds., Taylor and Francis Group, London, UK, 1611–1619.

Barron, R.A. (1948). "Consolidation of fine-grained soils by drain wells." *Transactions*, ASCE, **113**, 718–754.

Briaud, J.L. (2013). *Geotechnical Engineering, Unsaturated and Saturated Soils*. John Willy and Sons, New Jersey, USA.

Brinkgreve, R.B.J. and Vermeer, P.A. (2012). *PLAXIS: Finite Element Code for Soil and Rock Analyses*. Version 8.5, Balkema, Rotterdam.

Dash, S.K. and Bora, M.C. (2013). "Influence of geosynthetic encasement on the performance of stone columns floating in soft clay." *Canadian Geotechnical Journal*, **50**(7), 754–765.

Geng, L., Tang, L., Cong, S.Y., Ling, X.Z., and Lu, J. (2017). "Three-dimensional analysis of geosynthetic-encased granular columns for liquefaction mitigation." *Geosynthetics International*, **24**(1), 45–59.

Gniel, J. and Bouazza, A. (2010). "Construction of geogrid encased stone columns: A new proposal based on laboratory testing." *Geotextiles and Geomembranes*, **28**(1), 108–118.

Hatami, K. and Bathurst, R.J. (2005). "Development and verification of a numerical model for the analysis of geosynthetic reinforced-soil segmental walls." *Canadian Geotechnical Journal*, **42**(4), 1066–1085.

Hasan, M. and Samadhiya, N.K. (2016). "Experimental and numerical analysis of geosynthetic-reinforced floating granular piles in soft clays." *International Journal of Geosynthetics and Ground Engineering*, September, 2-22, https://doi.org/10.1007/s40891-016-0062-6.

Hosseinpour, I., Almeida, M.S.S., Riccio, M., and Baroni, M. (2017). "Strength and compressibility characteristics of a soft clay subjected to ground treatment." *Geotechnical and Geological Engineering*, **35**(3), 1051–1066.

Hosseinpour, I., Riccio, M., and Almeida, M.S.S. (2014). "Numerical evaluation of a granular column reinforced by geosynthetics using encasement and laminated disks." *Geotextiles and Geomembranes*, **42**(4), 363–373.

Hosseinpour, I., Almeida, M.S.S., and Riccio, M. (2015). "Full-scale load test and finite-element analysis of soft ground improved by geotextile-encased granular columns." *Geosynthetics International*, **22**(6), 428–438.

Khabbazian, M., Kaliakin, V.N., and Meehan, C.L. (2010). "Numerical study of the effect of geosynthetic encasement on the behaviour of granular columns." *Geosynthetics International*, **17**(3), 132–143.

Malarvizhi, S.N. and Ilamparuthi, K. (2007). "Comparative study on the behavior of encased stone column and conventional stone column." *Soils and Foundations*, JGS, **47**(5), 873–885.

Mirmoradi, S.H. and Ehrlich, M. (2015). "Modeling of the Compaction-induced stress on reinforced soil walls." *Geotextiles and Geomembranes*, **43**(1), 82–88.

Mitchell, J.K. and Huber, T.R. (1985). "Performance of stone column foundation." *Geotechnical Engineering*, ASCE, **111**(2), 205–223.

Murugesan, S. and Rajagopal, K. (2006). "Geosynthetic-encased stone column: Numerical evaluation." *Geotextiles and Geomembranes*, **24**(6), 349–358.

Murugesan, S. and Rajagopal, K. (2010). "Studies on the behavior of single and group of geosynthetic encased stone columns." *Geotechnical and Geoenvironmental Engineering*, ASCE, **136**(1), 129–139.

Raithel, M. and Henne, J. (2000). "Design and numerical calculation of a dam foundation with geotextile coated sand columns." *Proceeding of the 4th International Conference on Ground Improvement Geosystems*, 1–8.

Raithel, M., Kirchner, A., Schade, C., and Leusink, E. (2005). "Foundation of constructions on very soft soils with geotextile encased columns-state of the art." *Innovations in Grouting and Soil Improvement*, 1–11.

Rajesh, J. (2017). "Time-dependent behaviour of fully and partially penetrated geosynthetic encased stone columns." *Geosynthetics International*, **24**(1), 60–71.

Robertson, P.K. (2006). *Guide for In-Situ Testing*. Gregg Drilling & Testing, California, USA.

Tan, S.A., Tjahyono, S., and Oo, K.K. (2008). "Simplified plane-strain modeling of stone-columns reinforced ground." *Geotechnical and Geoenvironmental Engineering*, ASCE, **134**(2), 185–194.